NASA TECHNICAL MEMORANDUM

NASA TM X-3194

NASA TM X-3194

COMPARISON OF EXPERIMENTAL AND THEORETICAL BOUNDARY-LAYER SEPARATION FOR INLETS AT INCIDENCE ANGLE AT LOW-SPEED CONDITIONS

E. John Felderman and James A. Albers

Lewis Research Center

Cleveland, Ohio 44135

NATIONAL AERONAUTICS AND SPACE ADMINISTRATION • WASHINGTON, D. C. • FEBRUARY 1975

1. Report No. NASA TM X-3194	2. Government Accession No.	3. Recipient's Catalog No.
4. Title and Subtitle COMPARISON OF EXPERIMENTAL AND THEORETICAL BOUNDARY-LAYER SEPARATION FOR INLETS AT INCIDENCE ANGLE AT LOW-SPEED CONDITIONS		5. Report Date February 1975 6. Performing Organization Code
7. Author(s) E. John Felderman and James A. Albers		8. Performing Organization Report No. E-8182 10. Work Unit No. 505-05
9. Performing Organization Name and Address Lewis Research Center National Aeronautics and Space Administration Cleveland, Ohio 44135		11. Contract or Grant No. 13. Type of Report and Period Covered Technical Memorandum
12. Sponsoring Agency Name and Address National Aeronautics and Space Administration Washington, D.C. 20546		14. Sponsoring Agency Code

15. Supplementary Notes

16. Abstract

Comparisons between experimental and theoretical Mach number distributions and separation locations are presented for the internal surfaces of four different subsonic inlet geometries with exit diameters of 13.97 centimeters. The free stream Mach number was held constant at 0.127, the one-dimensional throat Mach number ranged from 0.49 to 0.71, and the incidence angle ranged from 0° to 50°. Generally good agreement was found between the theoretical and experimental surface Mach number distributions as long as no flow separation existed. At high incidence angles, where separation was obvious in the experimental data, the theory predicted separation on the lip. At lower incidence angles, the theoretical results indicated diffuser separation which was not obvious from the experimental surface Mach number distributions. As incidence angle was varied from 0° to 50°, the predicted separation location shifted from the diffuser region to the inlet highlight. Relatively small total pressure losses were obtained when the predicted separation location was greater than 0.6 of the distance between the highlight and the diffuser exit.

17. Key Words (Suggested by Author(s))	18. Distribution Statement
Inlet flow; Boundary layer separation; Engine inlet; Potential flow; Diffuser; Boundary layer flow	Unclassified - unlimited STAR category 02 (rev.)

19. Security Classif. (of this report)	20. Security Classif. (of this page)	21. No. of Pages	22. Price*
Unclassified	Unclassified	33	$3.75

* For sale by the National Technical Information Service, Springfield, Virginia 22151

COMPARISON OF EXPERIMENTAL AND THEORETICAL BOUNDARY-LAYER SEPARATION FOR INLETS AT INCIDENCE ANGLE AT LOW-SPEED CONDITIONS

by E. John Felderman* and James A. Albers

Lewis Research Center

SUMMARY

Comparisons between experimental and theoretical Mach number distributions and separation locations are presented for the internal surfaces of four different subsonic inlet geometries with exit diameters of 13.97 centimeters. The free stream Mach number was held constant at 0.127, the one-dimensional throat Mach number ranged from 0.49 to 0.71, and the incidence angle ranged from 0° to 50°. Generally good agreement was found between the theoretical experimental surface Mach number distributions as long as no flow separation existed. At high incidence angles, where separation was obvious in the experimental data, the theory predicted separation on the lip. At lower incidence angles, the theoretical results indicated diffuser separation which was not obvious from the experimental surface Mach number distributions. As incidence angle was varied from 0° to 50°, the predicted separation location shifted from the diffuser region to the inlet highlight. Relatively small total pressure losses were obtained when the predicted separation location was greater than 0.6 of the distance between the highlight and the diffuser exit.

INTRODUCTION

A problem in the development of subsonic aircraft engine nacelles is the design of efficient subsonic inlet diffusers which provide high total pressure recovery, low total pressure distortion, and uniform flow to the engine fan or compressor during low-speed and cruise operation. In general, the designer tries to avoid flow separation on the dif-

*Assistant Professor of Mechanical Engineering, South Dakota State University, Brookings, South Dakota; NASA Summer Faculty Fellow at the Lewis Research Center in 1974.

fuser surface to enhance the compatability between the inlet and engine. Most of the diffuser design guidelines presently available are empirical and are based on correlations of experimental data (e.g., ref. 1). Diffuser performance maps based on empirical correlations have been published by Reneau (ref. 2) for incompressible two-dimensional flow and by Sovran (ref. 3) for incompressible annular flow. More recent performance maps for compressible flow in straight channel diffusers can be found in references 4 and 5. These references indicate that diffuser performance is sensitive to diffuser entrance conditions such as Mach number and displacement thickness. However, these entrance conditions are determined from the lip geometry and flow conditions of the inlet. Thus, it is important for the analysis to consider both the inlet lip and diffuser when establishing design guidelines for the selection of separation-free diffuser geometries for engine inlets.

A previous investigation (ref. 6) established diffuser separation limits for use in subsonic inlet design. This was done using the calculation procedure developed by Albers and Stockman (ref. 7). In this study (ref. 6), a range of diffuser length-to-diameter ratios, diffuser area ratios, and diffuser contours was investigated. Based on theoretical predictions, separation boundaries were established.

The objective of this investigation is to provide experimental verification of the prediction of diffuser and/or lip separation. The experimental data were obtained from the work reported in reference 8. Comparisons between experimental and theoretical Mach number distributions and separation locations are made for four different inlet geometries at low speed (takeoff and landing) operating conditions. Comparisons are made on the windward side of the inlet for incidence angles from 0° to 50°. The free stream Mach number was held at a constant value of 0.127, with one-dimensional throat Mach numbers ranging from 0.49 to 0.71.

SYMBOLS

A flow area

a major axis of ellipse

b minor axis of ellipse

C_f skin friction coefficient

D diameter

L length

M Mach number

n superellipse exponent

P total pressure

q dynamic pressure

R radius

S nondimensional surface distance measured from stagnation point

s surface distance measured from highlight

u velocity in boundary layer

V velocity

X length of external forebody

α inlet incidence angle, angle between free stream velocity and inlet axis

β maximum wall angle

δ^* displacement thickness

$\theta/2$ equivalent conical half angle, arc tan $\left[\left(\sqrt{\frac{A_2}{\pi}} - \sqrt{\frac{A_t}{\pi}}\right)/L_d\right]$

ψ circumferential angle

Subscripts:

avg average

c centerbody

d diffuser

e edge of boundary layer

max maximum

ref surface reference distance from highlight to diffuser exit

sep separation location

t throat

0 tunnel

1 highlight

2 diffuser exit

∞ free stream

EXPERIMENTAL CONFIGURATIONS

A series of 13.97-centimeter-diameter inlets was tested in the Lewis Research Center's 9- by 15-foot V/STOL Propulsion Wind Tunnel (ref. 8). The tests were conducted at a free stream Mach number of 0.127 and inlet incidence angles ranging from 0° to 50°. Model instrumentation provided measurements of total pressure loss at the diffuser exit, inlet weight flow, and static pressure distributions on the internal surfaces of the inlet between the highlight and the diffuser exit (fig. 1). Surface Mach numbers were computed from these static pressure measurements assuming a constant total pressure (free stream value) throughout the inlet.

Four configurations were selected for the data-theory comparisons reported here. The first two configurations are shown in figure 2, and the important geometric variables for the four configurations are summarized in table I. Configuration 1, with the centerbody retracted, is shown in figure 2(a). Configuration 2 differs from 1 in that the centerbody is extended as shown in figure 2(b). The centerbody is also extended for configurations 3 and 4. Configuration 4 differs from 3 in that the inlet lip is nonsymmetric. The ratio of the highlight radius to the throat radius for configuration 4 is increased on the windward side ($\psi = 0^{\circ}$) of the inlet. The other important parameters for these inlet configurations, including the type of contours used for the internal lip and the external forebody, are listed in table I.

CALCULATION PROCEDURE

Overall Procedure

Theoretical calculations were carried out using four computer programs in the manner shown schematically in figure 3. The first program, SCIRCL, generates the coordinates and point-spacing on the inlet surfaces (ref. 9). The output from SCIRCL is fed directly into the second program, EOD, which is the Douglas axisymmetric incompressible potential flow program (ref. 10). The Douglas program is used to obtain three basic solutions for flow about inlets which are used as the input to a third computer program called COMBYN. It combines these basic solutions to obtain a solution for any combination of free stream velocity, inlet incidence angle, and mass flow rate through the inlet (ref. 11). COMBYN also corrects the incompressible potential flow solution for compressibility using the Lieblein-Stockman method described in reference 12.

The surface Mach number distributions for COMBYN are used as input to the fourth program, VISCUS. Program VISCUS (ref. 13) calculates the boundary layer growth and determines the separation point (if any) on the inlet surface. This calculation is axisymmetric, and any secondary flow due to the inlet being at angle of attack is neglected. The compressible boundary layer calculation proceeds from laminar flow (starting at the stagnation point) through transition into turbulent flow. Transition is predicted based on the empirical correlations of reference 14. Flow separation is indicated by zero wall shear stress and a sufficiently large shape factor. For turbulent flow in the diffuser, separation would occur at a shape factor greater than approximately 2.2.

Displacement Thickness Iteration

The first potential flow solution, as previously described (fig. 3), is carried out neglecting the boundary layer. In order to account for the presence of the boundary layer at a given circumferential location, it is necessary to add the displacement thickness at that circumferential location to the entire body and then recalculate the potential flow and boundary layer solution. This procedure would have to be continued in an iterative manner until convergence is obtained.

In order to demonstrate this procedure, displacement thicknesses were computed for configuration 1 as shown in figure 4. Results for the unseparated flow conditions from the first, second, and third computations in the iteration are shown in figure 4(a). The deviation between the first and second iteration indicates that at least another iteration would be required for convergence. Since the displacement thickness changes only slightly between the second and third iterations, it was concluded that the second computation is a reasonable approximation to the converged result. Also, very good agreement between experimental data and predicted surface Mach number distributions were obtained in the past with this approximation (refs. 15 and 16).

When separation is predicted, the iterative procedure to account for displacement thickness is not as straightforward. Figure 4(b) shows the displacement thickness for an example of this type. As before, the boundary layer is neglected when carrying out the first potential flow computation. Using the potential flow solution, the first boundary layer solution is carried as far as the separation point where it then breaks down. However, before the second potential flow solution can be carried out, the displacement thickness must be added to the body along the entire length of the diffuser. Since it is known only up to the separation point, it must be extrapolated to the diffuser exit. Since the slope of the displacement thickness curve is increasing rapidly just prior to separation, it is not obvious how to make the correct extrapolation. The extrapolation shown

in figure 4(b) was made using the attached flow results (fig. 4(a)) as a guide to the general shape of the curve. A second computation was made using this extrapolation of the first computation. The deviation between the results from the first and second computations are of approximately the same relative magnitude as for the attached case (fig. 4(a)) up to the point of separation. As with the attached flow conditions, the second computation is considered to be a reasonable approximation to the converged result. However, the displacement thickness correction up to the separation point may be sensitive to errors in the estimated effective displacement thickness after separation. Because of the large computer time required, the second computation was not done in all cases.

The theoretical Mach number distributions obtained for the separated cases does not reflect the true separated distribution from the separation point to the diffuser exit. Instead, because of the displacement thickness extrapolation technique just described, the distribution is probably a better representation of what the distribution would have been had the flow remained attached.

When separation occurs, the flow is no longer axisymmetric and large separated and secondary flows could exist within the inlet at high incidence angles. The effect of secondary flow on the flow solution is not considered in this analysis. However, when large separated regions and large secondary flows do not exist in the inlet, the axisymmetric solution is probably a good approximation to the three-dimensional flow.

DISCUSSION OF RESULTS

Experimental Total Pressure Recovery

The experimental total pressure recovery indicates the overall aerodynamic performance of the inlet. Area-weighted pressure recoveries as a function of incidence angle for the four inlet configurations studied are shown in figure 5 for a free stream Mach number of 0.127 at various one-dimensional throat Mach numbers. The pressure recovery was above around 0.99 for configurations 1, 3, and 4, for inlet incidence angles of 0°, 20°, 30°, and 40°. A rapid drop in pressure recovery to a level below 0.96 occurred at an incidence angle of 50° for configurations 1, 2, and 3. Reference to these recovery levels will be made in subsequent discussions when comparing experimental and predicted separation locations.

Experimental and Theoretical Mach Number Distributions and Separation Locations

Comparisons of experimental and theoretical surface Mach numbers are shown as a function of nondimensional surface distance measured from the highlight on the windward

side of the inlet ($\psi = 0^{\circ}$) in figures 6 and 9 to 13. Predicted separation locations are also indicated on the figures. Comparisons of data and theory are presented for the four inlet configurations discussed previously, for five values of the inlet incidence angle (0°, 20°, 30°, 40°, and 50°), and for a range of one-dimensional throat Mach numbers from 0.49 to 0.71. All comparisons are at a free stream Mach number M_{∞} of 0.127. Also shown are experimental velocity profiles obtained from rake total pressure measurements at the diffuser exit.

Centerbody retracted configuation. - Results for a one-dimensional throat Mach number $M_t = 0.496$ are shown in figure 6. At zero incidence angle (fig. 6(a)), there is very good agreement between data and theory, especially when the δ^* correction is made. No separation is predicted theoretically, nor is any observed experimentally. At the higher incidence angles, diffuser separation is predicted (figs. 6(b) to (d)). Agreement between experimental and theoretical Mach number distributions is relatively good up to the separation prediction point. After the separation point, the theory begins to deviate from the data with the deviation increasing with incidence angle. The "pressure plateau" commonly associated with an experimentally observed separation is not fully evident until an incidence angle of 40° is reached.

At an incidence angle of 50°, separation is predicted in the laminar region not far from the highlight (fig. 6(e)). Experimentally, the flow appears to be separated at the highlight. This difference between the predicted and experimental separation location may be a result of an inaccuracy in the prediction of the boundary layer transition point or the effect of the downstream separation on the upstream static pressure distribution. A small inaccuracy in predicting the transition location has an important effect on whether or not lip separation is predicted.

Since the predicted surface Mach number distributions and separation location shifts downstream only slightly with the δ^* correction, the first computation (without δ^*) is a reasonable approximation to the solution. This will result in a conservative estimate of the separation location. Therefore, displacement thickness corrections were performed for only some of the remaining configurations because of the large computation time required to make this correction.

Examination of the velocity profiles obtained from the rake total pressure measurements shown in figure 6 indicate an increasing defect in the velocity as incidence angle increases. At incidence angles of 40° and below, there is not enough total pressure measurements to make a positive determination concerning separation. However, at a 50° incidence angle inspection of the velocity profile indicates separation.

The surface Mach number distributions and velocity profiles shown in figure 6 are for the windward side ($\psi = 0^{\circ}$) of the inlet. The inlet loss behavior at other radial positions can be seen from the pressure recovery contour plots of figure 7. At $\alpha = 20^{\circ}$, a small local region of loss is noted at the bottom of the inlet (windward side). The loss

increases in magnitude and spreads radially and circumferentially with increasing incidence angle. At $\alpha = 50^{\circ}$, a large separated region is observed on the windward side of the inlet.

The effect of increasing incidence angle on the overall inlet performance of configuration 1 can also be seen from the pressure recoveries plotted in figure 5(a). The pressure recovery is very nearly unity at zero incidence angle indicating attached flow. As incidence angle increases, the pressure recovery drops. The lip separation experienced at $\alpha = 50^{\circ}$ results in a very substantial drop in pressure recovery to below 0.95.

The shift in separation location and severity of separation can be further illustrated by examination of the theoretical local skin friction coefficient. The local skin friction coefficient shown in figure 8 is plotted from the stagnation point on the inlet lip. The inlet highlight and throat locations are also noted on the figure. Examination of the figure indicates two regions on the inlet surface where separation is more likely, that is, regions where the friction coefficient has a minimum and a low value. One region is on the inlet lip and the other is in the diffuser. The minimum skin friction point in the diffuser ($S \approx 0.6$) moves forward by only a relatively small amount, while the minimum point on the inlet lip ($S \approx 0.2$) remains about the same as incidence angle is increased. At an incidence angle of 50° the separation point ($C_f = 0$) shifts abruptly from the diffuser location to the inlet lip, as was also illustrated by the experimental pressure recovery contours of figure 7. The value of $s/s_{ref} = 0.6$ represents the middle of the diffuser.

Centerbody extended short diffuser (configuration 2). - Results for a one-dimensional throat Mach number of 0.707 are presented in figure 9. Separation is predicted for this configuration even for zero incidence angle (fig. 9(a)). Diffuser separation is predicted for all incidence angles up to and including 40°. Lip separation is predicted and observed experimentally at $\alpha = 50^{\circ}$.

Some discrepancy is noted between the Mach number data and theory in the region following the inlet highlight. The data falls below the theory especially at incidence angles of 20°, 30°, and 40° (figs. 9(b), (c), and (d)). This discrepancy may be due to a local separation bubble and/or by shock boundary layer interaction effects, or to the transition prediction.

Results for a one-dimensional throat Mach number M_t of 0.576 are shown in figure 10. A δ^* correction was made for configuration 2 for zero incidence angle. It can be seen that the predicted Mach number distribution and the separation location are not significantly changed. The correction to the surface Mach number distribution decreases the discrepancy between the data and the theory in the aft end of the diffuser at that angle. Relatively good comparison is also at an incidence angle of 20°. At 40°, diffuser separation is predicted theoretically but the pressure plateau is observed ex-

perimentally to start at the throat farther upstream than predicted. This deviation between data and theory is different than previously observed (fig. 6(d)). This is also reflected in the pressure recovery level of 0.98 (fig. 5(b)). Complete lip separation is again predicted and observed experimentally at an incidence angle of 50°.

Centerbody extended, long diffuser (configuration 3). - Results for configuration 3 with a throat Mach number M_t of 0.656 are presented in figure 11. No separation is predicted for zero incidence angle (fig. 11(a)), diffuser separation is predicted for $\alpha = 20^{\circ}$, 30°, and 40°, and lip separation is predicted for $\alpha = 50^{\circ}$ (fig. 11(e)). Examination of the experimental boundary layer profiles indicate separation flow at the diffuser exit at incidence angle of 50°, which is reflected in the decrease in pressure recovery at this incidence angle shown in figure 5(c). Although it is not clear from figure 11 where the separation actually starts, the pressure plateau is seen to start at the throat.

Centerbody extended, thicker lower lip (configuration 4). - Experimental results for configuration 4 with a nonsymmetric lip are shown in figures 12 and 13 for throat Mach numbers of 0.534 and 0.664 respectively. Theoretical calculations for this configuration were carried out assuming an axisymmetric inlet having the surface contour of the windward side ($\psi = 0^{\circ}$) of the inlet. No separation is predicted at 0° or 20° incidence angle for the lower throat Mach number (figs. 12(a) and (b)) nor for 0° incidence angle at the higher throat Mach number (fig. 13(a)). Experimental separation was not clearly evident at any incidence angle. However, a pressure plateau did exist at an incidence angle of 50°.

Summary of Separation Locations and Pressure Losses

A summary plot of separation locations as a function of inlet incidence angle is shown in figure 14 for all configurations. As incidence angle increases from 0° to 50°, the separation location shifts from the diffuser to the inlet highlight (complete lip separation). At 50° incidence angle, the experimental lip separation locations (figs. 14(a) and (b)) obtained from the static pressure plateau agrees well with the theoretical lip separation location. Relatively good agreement in separation location is also obtained at incidence angles of 30° and 40° (fig. 14(a)).

The total pressure loss of the configurations as a function of the separation locations is presented in figure 15. The total pressure loss increases as the separation location moves from the diffuser exit to the inlet highlight. Relatively small pressure losses were obtained when the predicted separation location (s/s_{ref}) was greater than 0.6. The moderate pressure loss associated with separation locations greater than 0.6 indicate that some separation could be tolerated in an inlet design provided total pressure distor-

tion levels are acceptable. However, inlet lip separation produces excessive losses and distortion.

SUMMARY OF RESULTS

Comparisons between experimental and theoretical Mach number distributions and separation locations were made for four different inlet geometries. Comparisons were made on the windward side of the inlet for a constant free stream Mach number of 0.127. The incidence angle was varied from 0° to 50°. One-dimensional throat Mach numbers in the range 0.49 to 0.71 were considered. The principal results of this study can be summarized as follows:

1. In general, good agreement was obtained between theoretical and experimental surface Mach number distributions as long as no flow separation existed.

2. As incidence angle increases from 0° to 50°, the predicted separation location shifted from about the middle of the diffuser to the inlet highlight (complete lip separation).

3. At high incidence angles where lip separation was obvious in the experimental data, the theory predicted separation. At lower incidence angles the theoretical results indicated separation on the diffuser surface which was not always obvious from the experimental profiles.

4. The total pressure loss increased as the separation location moved from the diffuser to the inlet highlight. Relatively small pressure losses were obtained when the predicted separation location was greater than 0.6 of the distance from the highlight to the diffuser exit.

Lewis Research Center,
National Aeronautics and Space Administration,
Cleveland, Ohio, December 16, 1974,
505-05.

REFERENCES

1. Henry, John R.; Wood, Charles C.; and Wilbut, Stafford W.: Summary of Subsonic-Diffuser Data. NACA RM L56F05, 1956.

2. Reneau, L. R.; Johnston, J. P.; and Kline, S. J.: Performance and Design of Straight, Two-Dimensional Diffusers J. Basic Eng., Trans. ASME, Ser. D, vol. 89, no. 1, Mar. 1967, pp. 141-150.

3. Sovran, Gino; and Klomp, Edward D.: Experimentally Determined Optimum Geometries for Rectilinear Diffusers with Rectangular, Conical or Annular Cross-Section. Symposium on the Fluid Mechanics of Internal Flow. G. Sovran ed., Elsevier Publishing Company (Amsterdam), 1962, pp. 270-319.

4. McMillan, O. J.; and Johnston, J. P.: Performance of Low-Aspect-Ratio Diffusers with Fully Developed Turbulent Inlet Flows. Part I - Some Experimental Results. ASME Paper 73-FE-12, July 1973.

5. Runstadler, P. W. Jr.; and Dolan, F. X.: Further Data on the Pressure Recovery Performance of Straight-Channel, Plan-Divergence Diffusers at High Subsonic Mach Numbers. ASME Paper 73-FE-5, July 1973.

6. Albers, James A.; and Felderman, E. John: Boundary-Layer Analysis of Subsonic Inlet Diffuser Geometries for Engine Nacelles. NASA TN D-7520, 1974.

7. Albers, J. A.; and Stockman, N. O.: Calculation Procedures for Potential and Viscous Flow Solutions for Engine Inlets. ASME Paper 74-GT-3, Mar.-Apr. 1974.

8. Abbott, John: Aero Acoustic Performance of Scale Model Sonic Inlets. AIAA Paper 75-202, Jan. 1975.

9. Stockman, Norbert O.; and Button, Susan L.: Computer Programs for Calculating Potential Flow in Propulsion System Inlets. NASA TM X-68278, 1973.

10. Hess, J. L.; and Smith, A. M. O.: Calculation of Potential Flow About Arbitrary Bodies. Progress in Aeronautical Sciences. Vol. 8, D. Kuchemann, ad., Pergamon Press, 1967, pp. 1-138.

11. Stockman, Norbert O.: Potential Flow Solutions for Inlets of VTOL Lift Fans and Engines. Analytic Methods in Aircraft Aerodynamics, NASA SP-228, 1970, pp. 659-681.

12. Lieblein, S.; and Stockman, N. O.: Compressibility Correction for Internal Flow Solutions. J. Aircraft, vol. 9, no. 4, Apr. 1972, pp. 312-313.

13. Albers, James A.; and Gregg, John L.: Computer Program for Calculating Laminar, Transitional, and Turbulent Boundary Layers for a Compressible Axisymmetric Flow. NASA TN D-7521, 1974.

14. Schlichting, Herman (J. Kestin trans.): Boundary Layer Theory. 6th ed., McGraw-Hill Book Co., Inc., 1968, pp. 431-516.

15. Albers, James A.: Theoretical and Experimental Internal Flow Characteristics of a 13.97-Centimeter-Diameter Inlet at STOL Takeoff and Approach Conditions. NASA TN D-7185, 1973.

16. Albers, J. A.: Comparison of Predicted and Measured Low-Speed Performance of Two 51-Centimeter-Diameter Inlets at Incidence Angle. NASA TM X-2937, 1973.

TABLE I. - GEOMETRIC VARIABLES FOR THE FOUR INLET CONFIGURATIONS CONSIDERED FOR THIS INVESTIGATION

[Inlet maximum diameter, 13.97 cm; centerbody diameter to exit diameter ratio, D_c/D_2, 0.364.]

Description	Centerbody retracted (configuration 1)	Centerbody extended, short diffuser (configuration 2)	Centerbody extended, long diffuser (configuration 3)	Centerbody extended, thicker lower lip (configuration 4)
Diffuser				
Ratio of length to exit diameter, L_d/D_2	0.425	0.425	0.607	0.607
Ratio of exit flow area to throat flow area, A_2/A_t	1.09	1.30	1.30	1.30
Maximum local wall angle in diffuser, β, deg	13.6	13.6	9.3	9.3
Equivalent diffuser conical half angle, $\theta/2$, deg	2.5	7.5	5.3	5.3
Internal lip				
Ratio of highlight radius to throat radius, R_1/R_t	1.14	1.14	1.14	[a]1.14 [b]1.20
Contour	Ellipse (n = 2)	Ellipse (n = 2)	Ellipse (n = 2)	Ellipse (n = 2)
Ratio of major to minor axis, a/b	2.0	2.0	2.0	[a]2.9 [b]2.0
External forebody				
Ratio of highlight radius to maximum radius, R_1/R_{max}	0.866	0.866	0.866	[a]0.866 [b].912
Ratio of length to maximum diameter, X/D_{max}	.30	.30	.30	[a].20 [b].30
Contour	NACA-1 Superellipse (n = 1.78)	NACA-1 Superellipse (n = 1.78)	NACA-1 Superellipse (n = 1.78)	Ellipse (n = 2)
Centerbody				
Ratio of length to exit diameter, L_c/D_2	0.364	0.789	0.971	0.971
Contour	Superellipse (n = 1.78)	Superellipse (n = 1.78)	Superellipse (n = 1.78)	Superellipse (n = 1.78)

[a]Circumferential angle, ψ, 180°; leeward side of inlet.
[b]Circumferential angle, ψ, 0°; windward side of inlet.

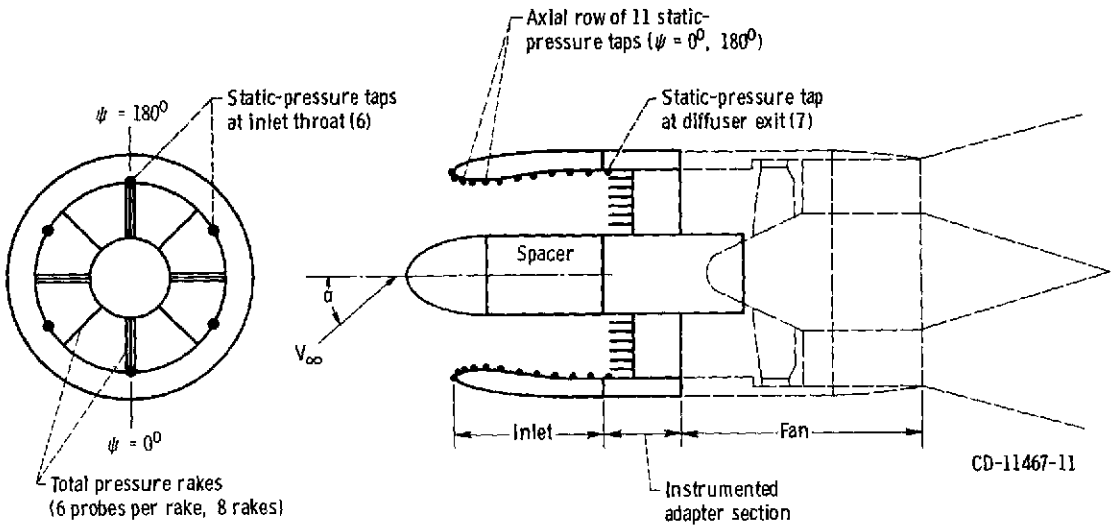

Figure 1. - Schematic view of test model showing location of instrumentation.

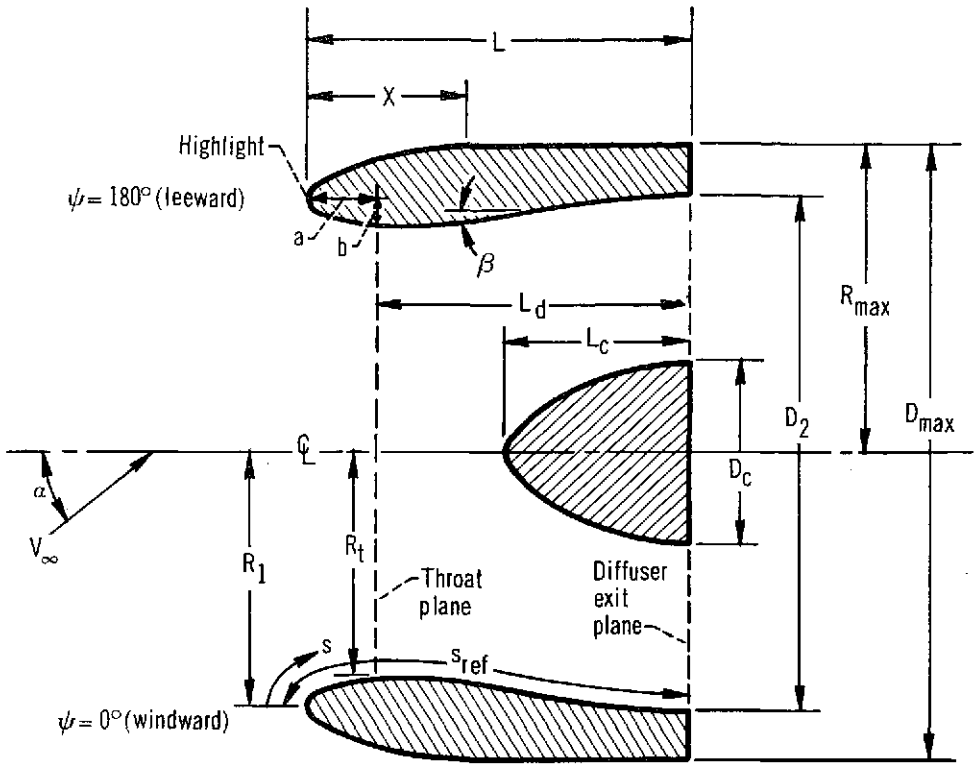

(a) Centerbody retracted (configuration 1).

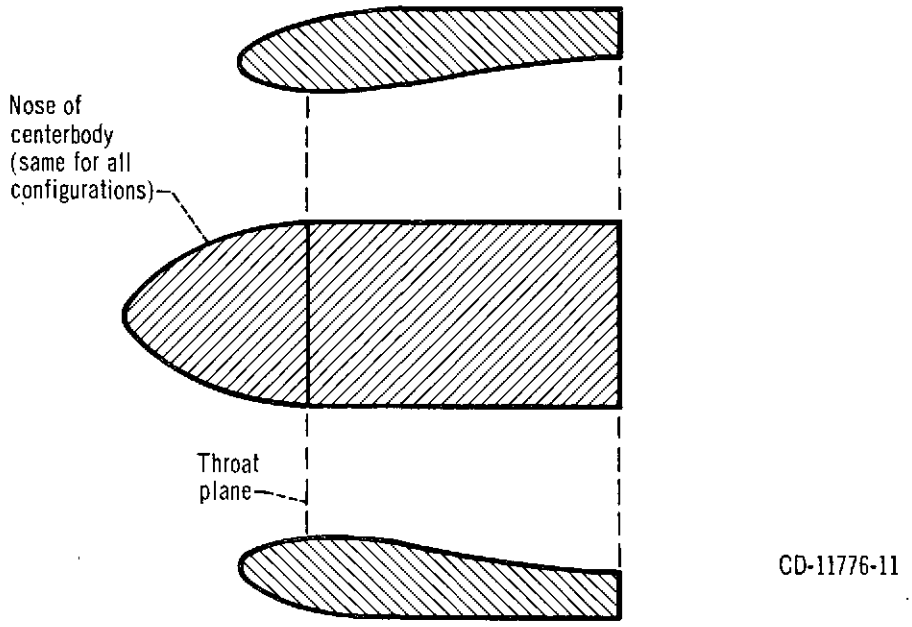

(b) Centerbody extended (configurations 2, 3, and 4).

Figure 2. - Illustration of inlet geometries.

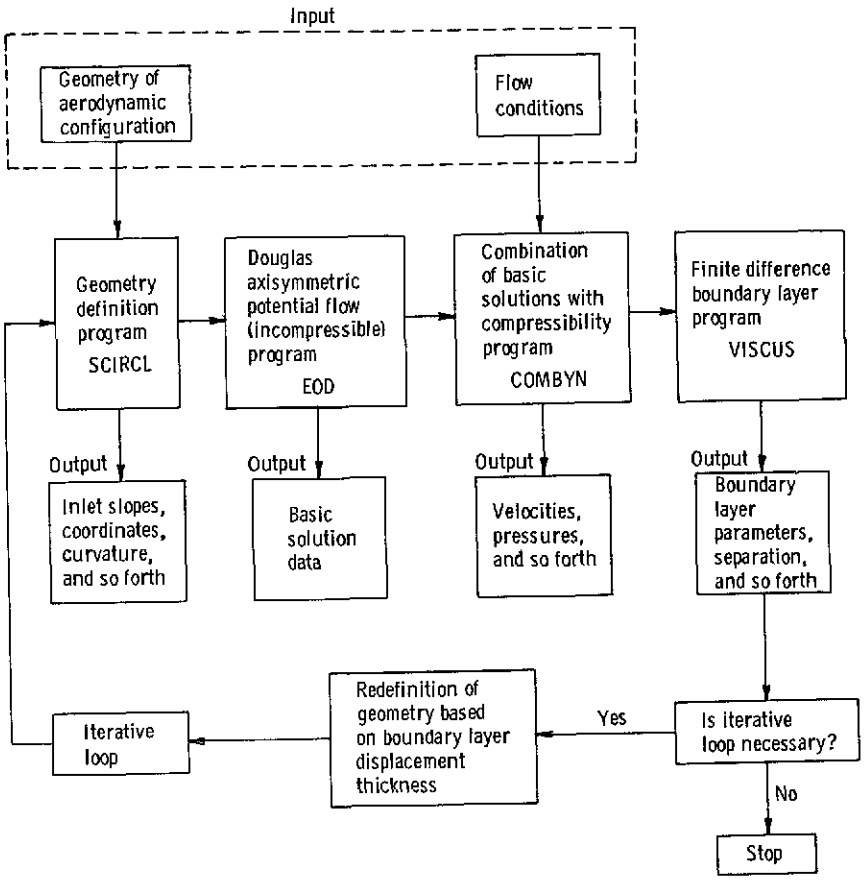

Figure 3. - Schematic of calculation procedure.

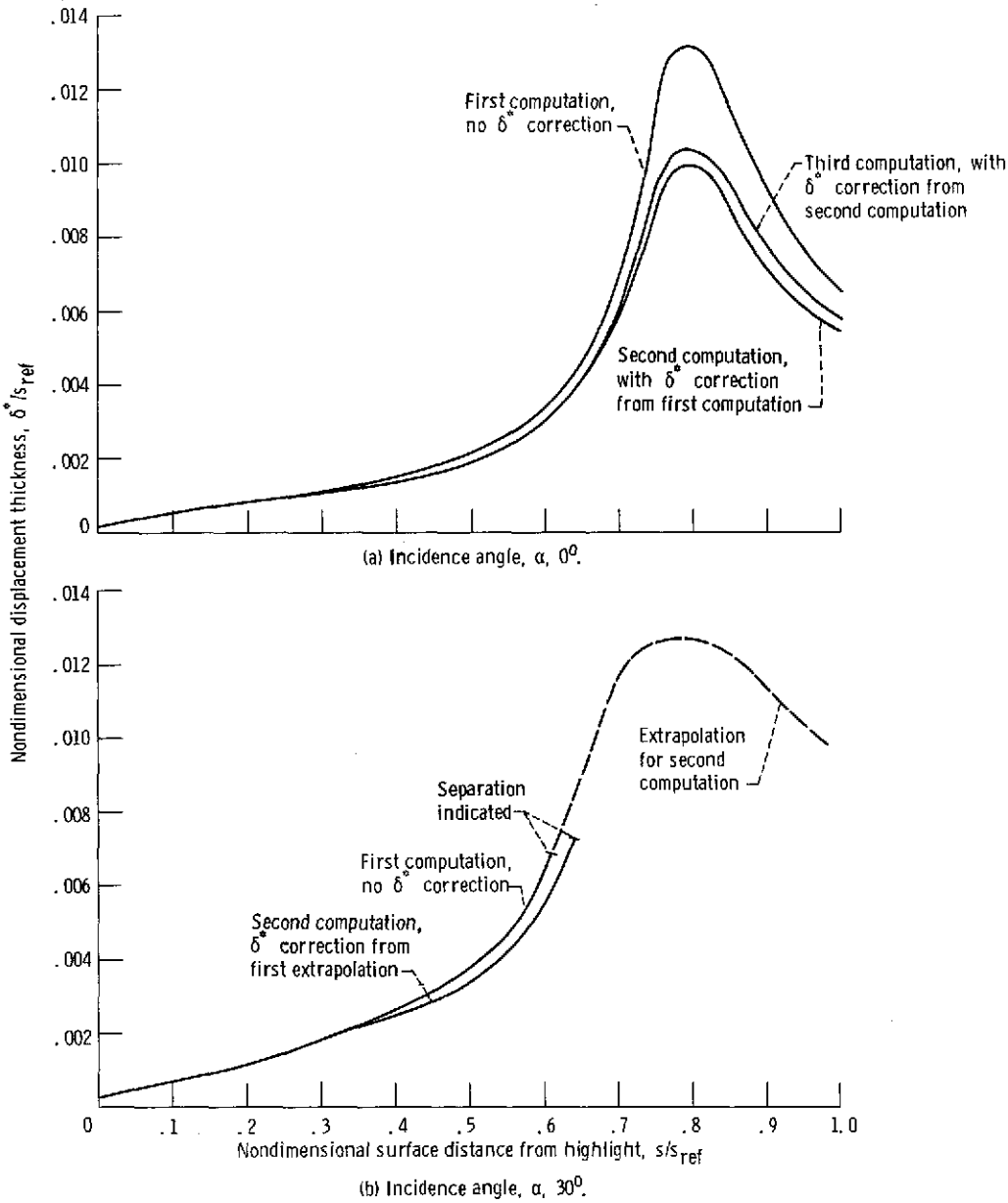

Figure 4. - Displacement thicknesses computed at various stages in inviscid-viscous iteration. Centerbody retracted; $\theta/2 = 2.5^\circ$ (configuration 1); one-dimensional throat Mach number, M_t, 0.496; free stream Mach number, M_∞, 0.127; windward side of inlet.

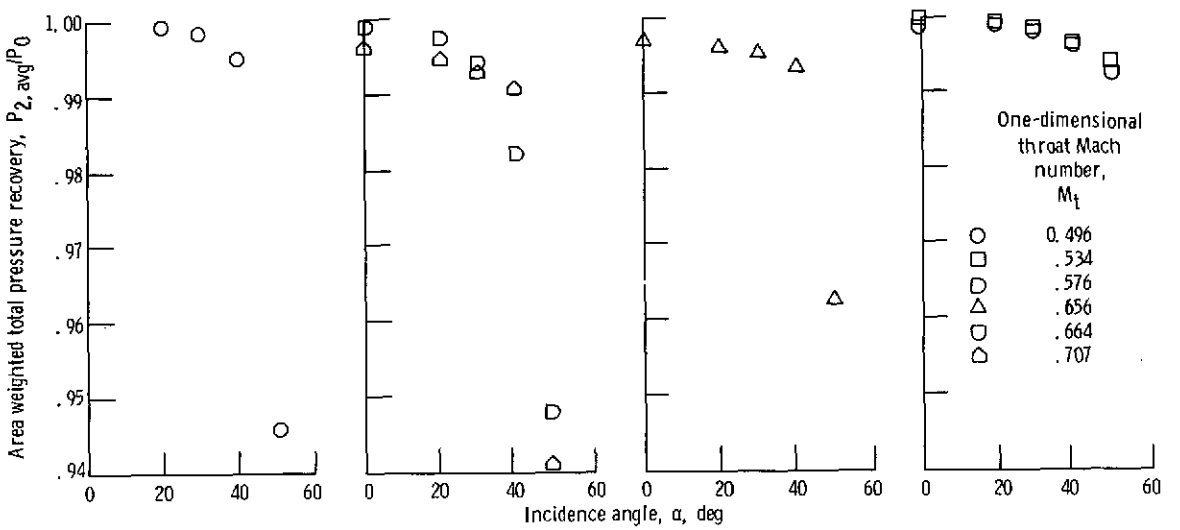

(a) Centerbody retracted; $\theta/2 = 2.5^0$ (configuration 1).

(b) Centerbody extended, short diffuser; $\theta/2 = 7.5^0$ (configuration 2).

(c) Centerbody extended, long diffuser; $\theta/2 = 5.3^0$ (configuration 3).

(d) Centerbody extended, nonsymmetric lip; $\theta/2 = 5.3^0$ (configuration 4).

Figure 5. - Experimental total pressure recovery for four inlet configurations considered. Free stream Mach number, M_∞, 0.127.

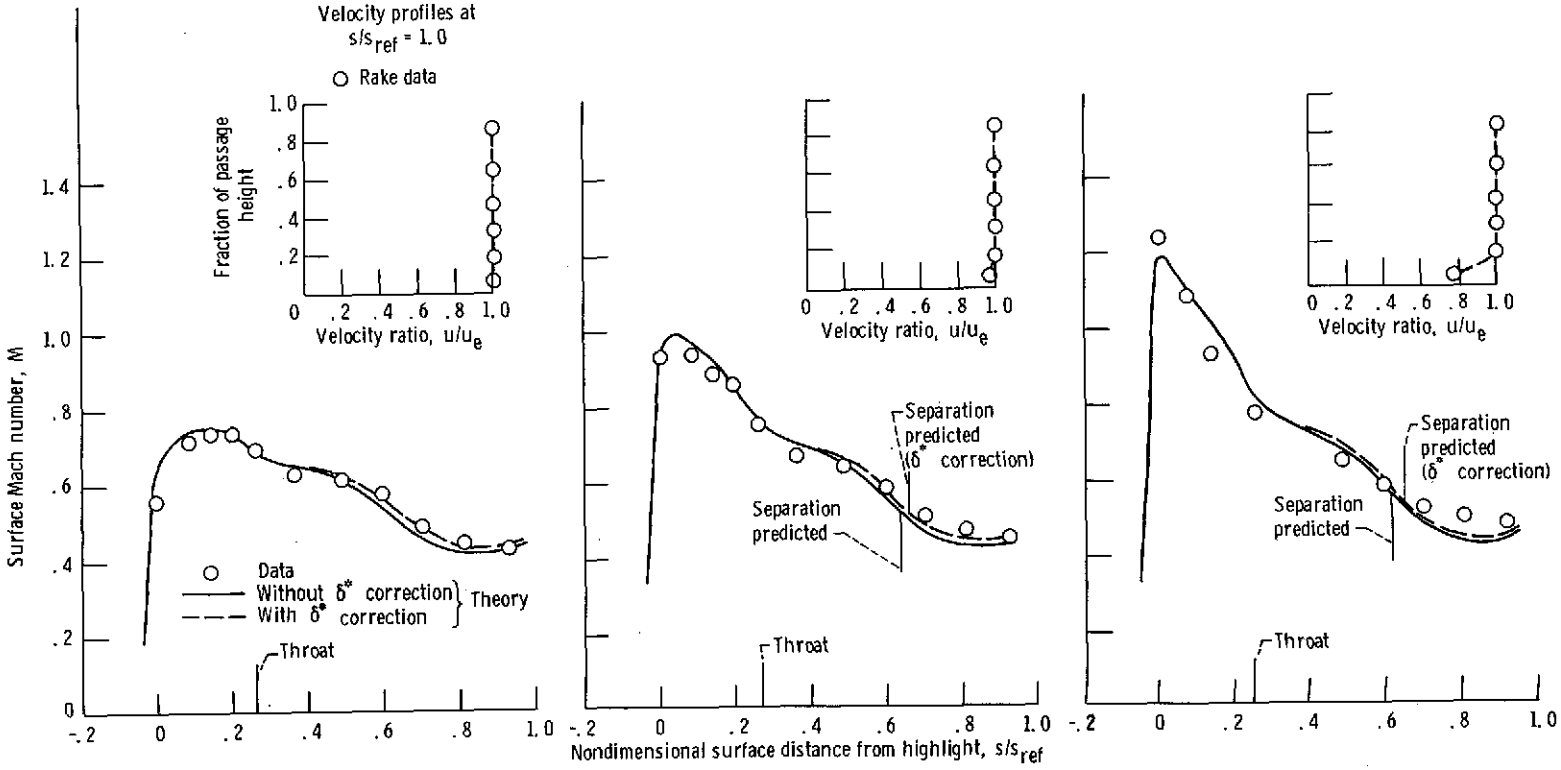

Figure 6. - Experimental and theoretical Mach number distributions and separation locations for centerbody retracted, $\theta/2 = 2.5^\circ$ (configuration 1). One-dimensional throat Mach number, M_t, 0.496; free stream Mach number, M_∞, 0.127; windward side of inlet.

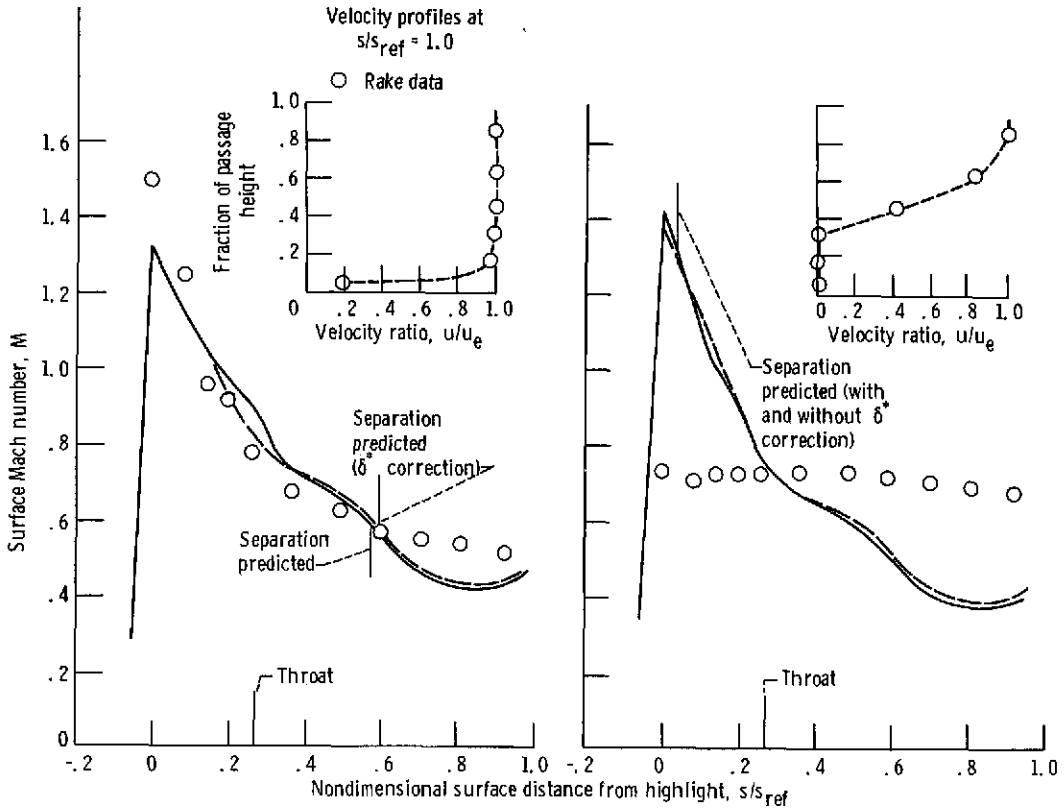

(d) Incidence angle, α, 40°.

(e) Incidence angle, α, 50°.

Figure 6. - Concluded.

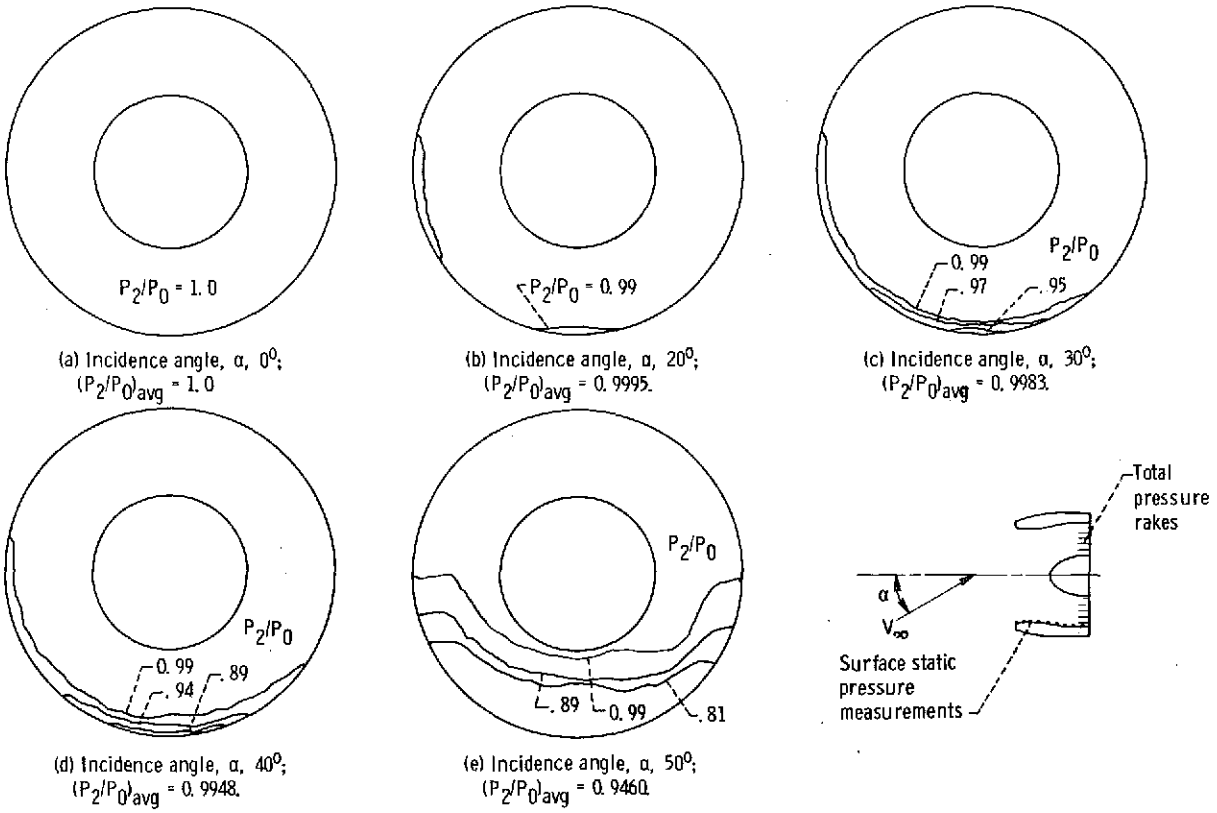

Figure 7. - Pressure recovery contour plots at diffuser exit for centerbody retracted; $\theta/2 = 2.5^\circ$ (configuration 1). One-dimensional throat Mach number, M_t, 0.496; free stream Mach number, M_∞, 0.127.

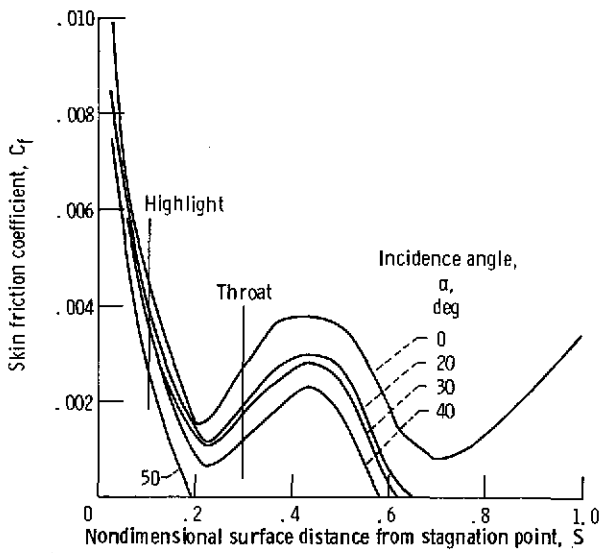

Figure 8. - Theoretical skin friction coefficients (without δ^* correction) for centerbody retracted; $\theta/2 = 2.5^\circ$ (configuration 1). One-dimensional throat Mach number, M_t, 0.496; free stream Mach number, M_∞, 0.127; windward side of inlet.

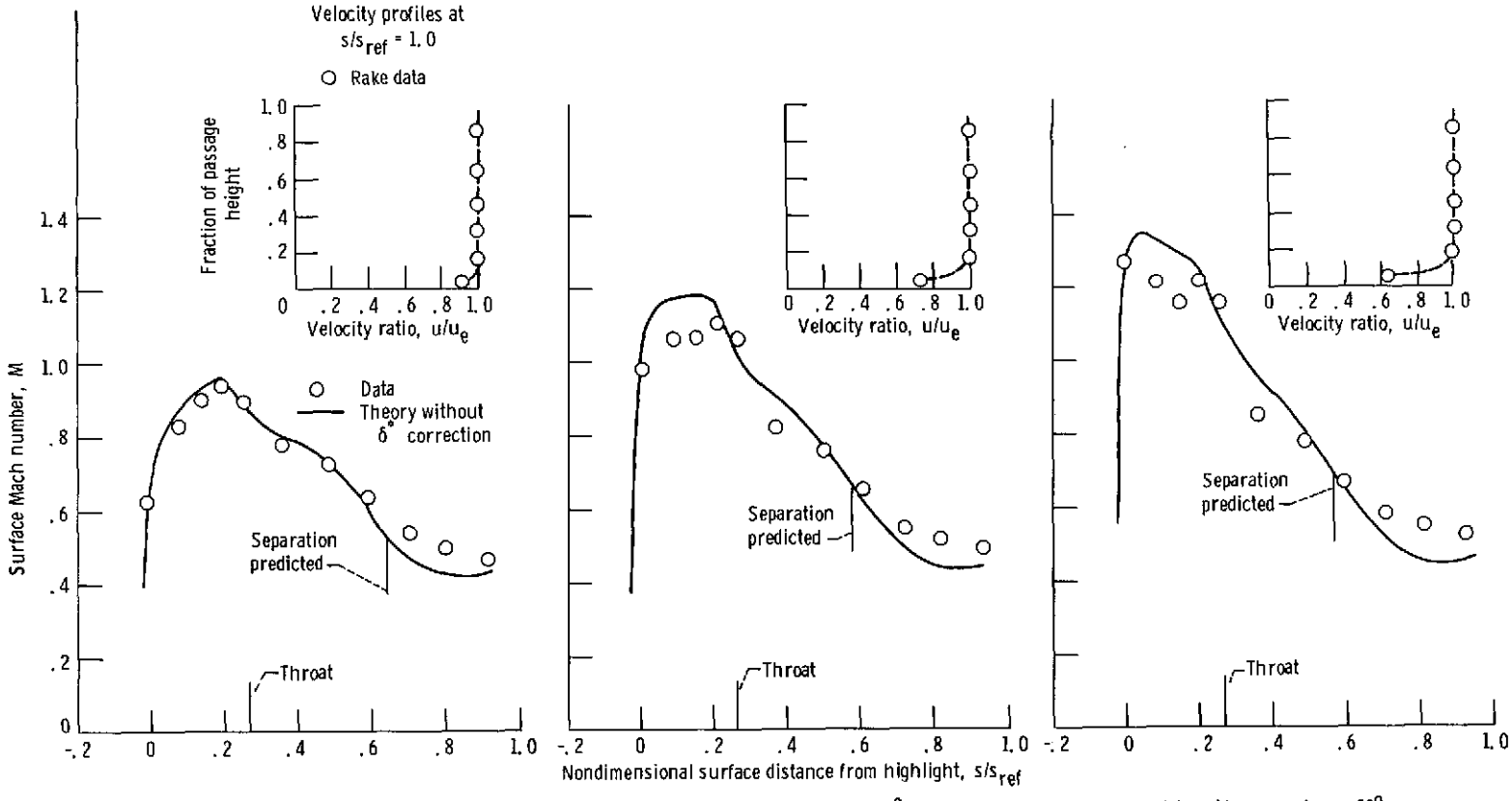

(a) Incidence angle, α, 0°. (b) Incidence angle, α, 20°. (c) Incidence angle, α, 30°.

Figure 9. - Experimental and theoretical Mach number distributions and separation locations for centerbody extended, short diffuser; θ/2 = 7.5° (configuration 2). One-dimensional throat Mach number, M_t, 0.707; free stream Mach number, M_∞, 0.127; windward side of inlet.

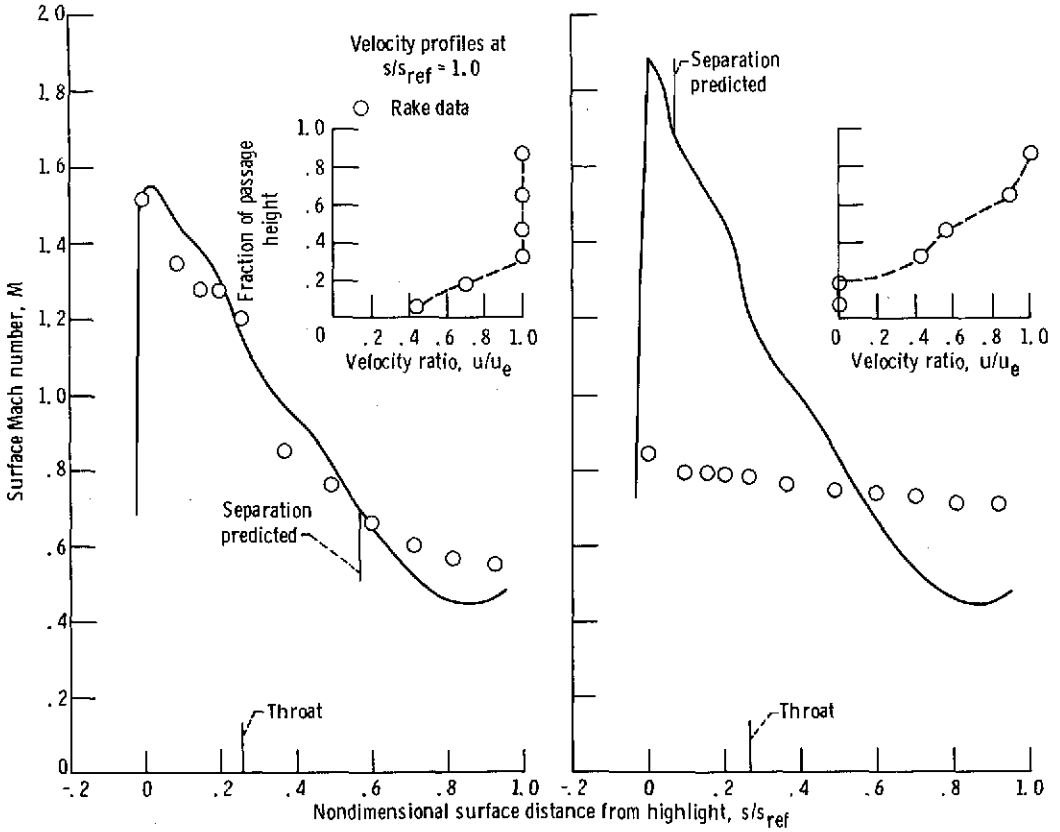

(d) Incidence angle, α, 40^0.

(e) Incidence angle, α, 50^0.

Figure 9. - Concluded.

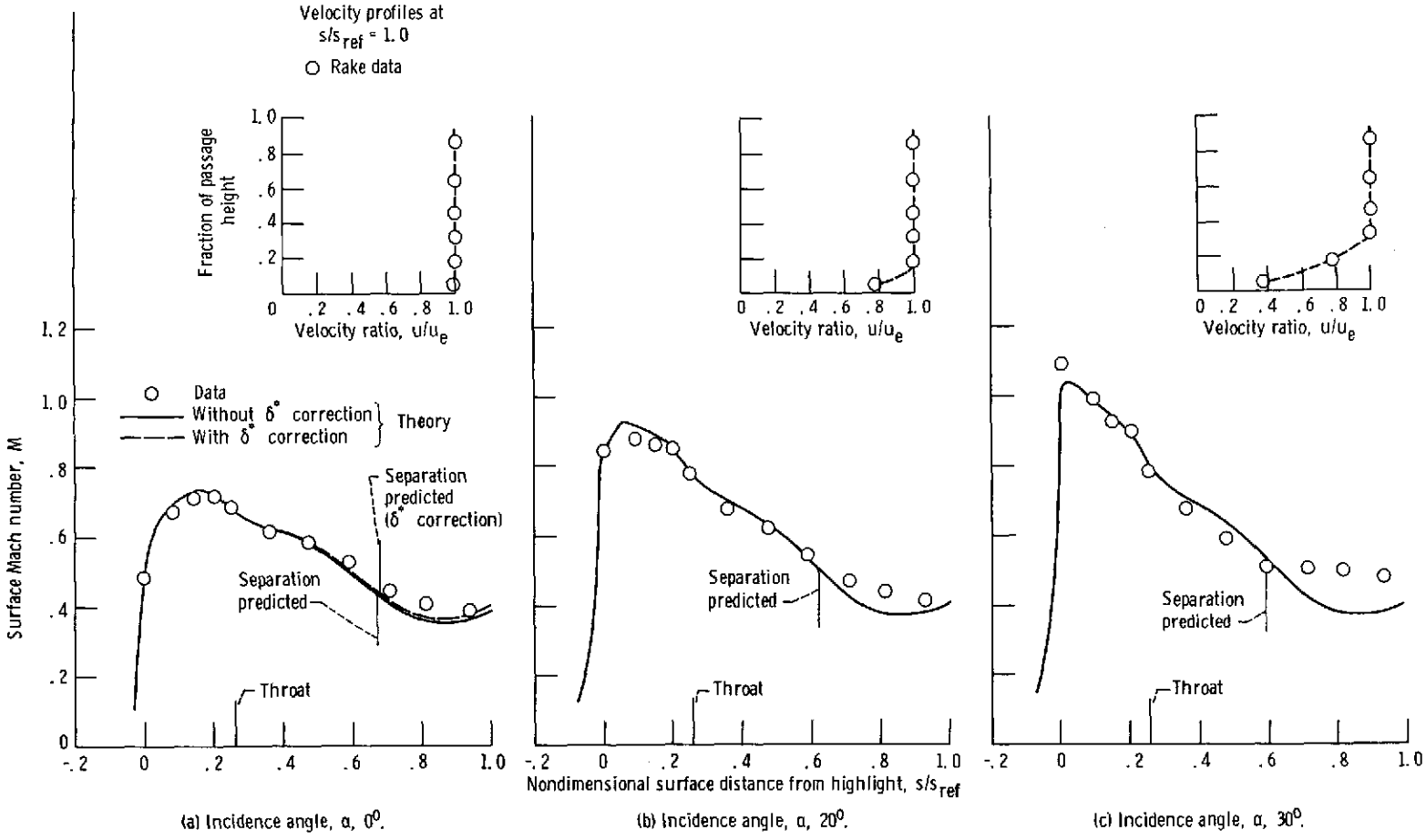

Figure 10. - Experimental and theoretical Mach number distributions and separation locations for centerbody extended, short diffuser; $\theta/2 = 7.5^0$ (configuration 2). One-dimensional throat Mach number, M_t, 0.576; free stream Mach number, M_∞, 0.127; windward side of inlet.

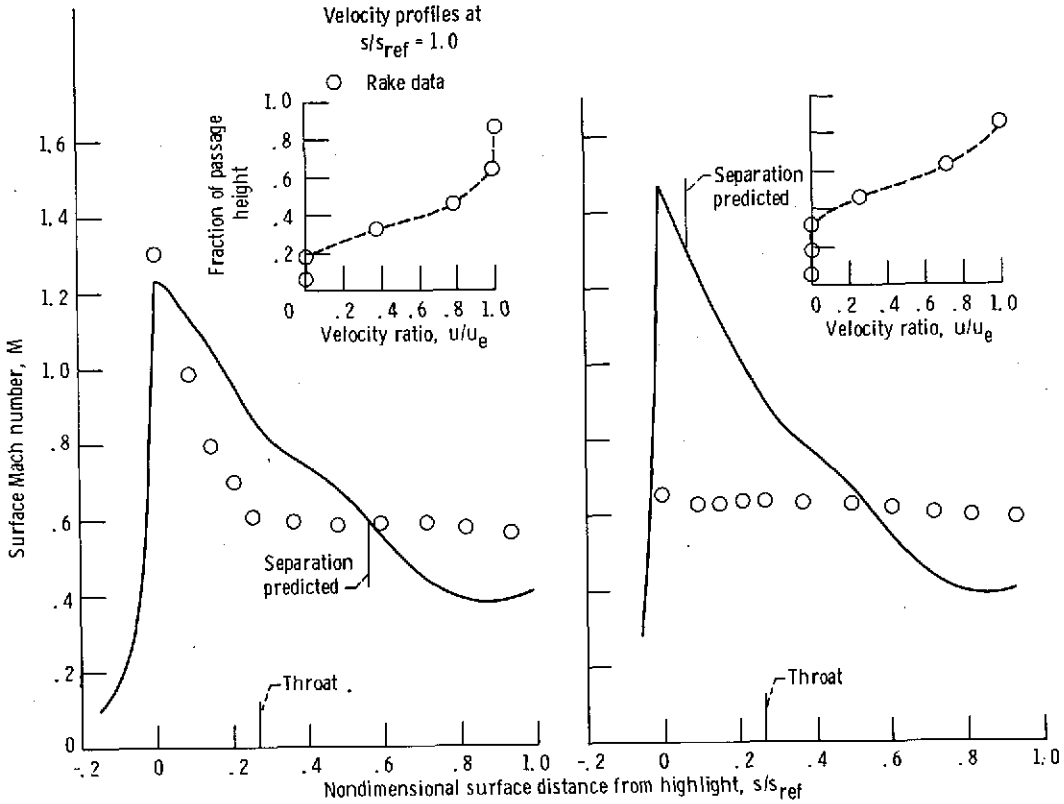

(d) Incidence angle, α, 40°.

(e) Incidence angle, α, 50°.

Figure 10. - Concluded.

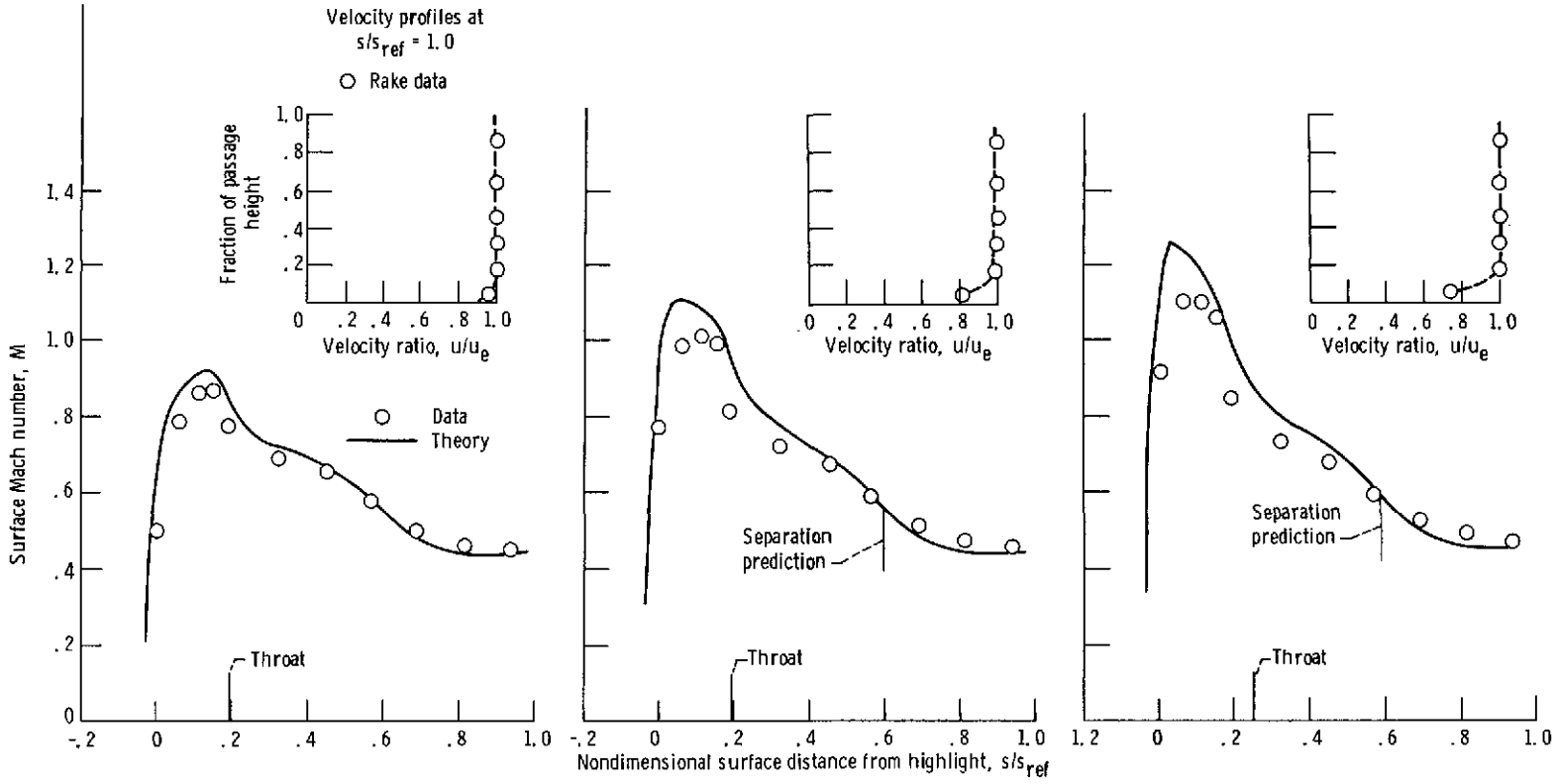

(a) Incidence angle, α, 0°. (b) Incidence angle, α, 20°. (c) Incidence angle, α, 30°.

Figure 11. - Experimental and theoretical Mach number distributions and separation locations for centerbody extended, long diffuser; θ/2 = 5.3° (configuration 3). One-dimensional throat Mach number, M_t, 0.656; free stream Mach number, M_∞, 0.127; windward side of inlet.

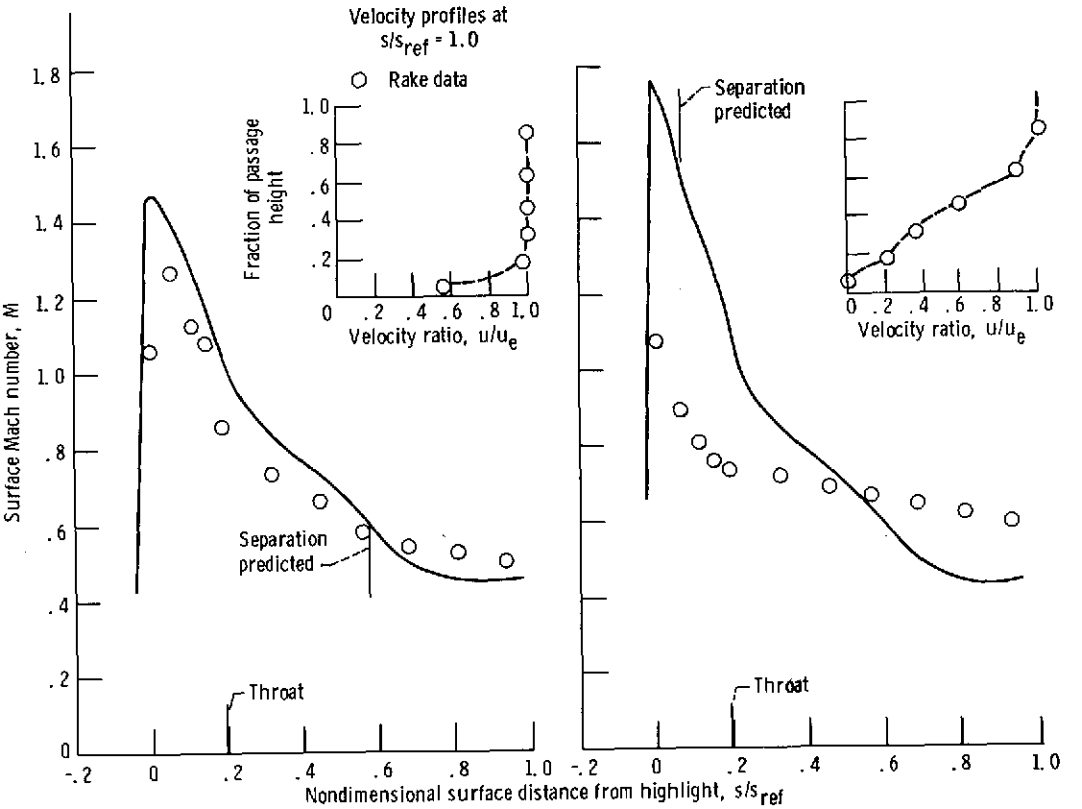

(d) Incidence angle, α, 40^0.

(e) Incidence angle, α, 50^0.

Figure 11. - Concluded.

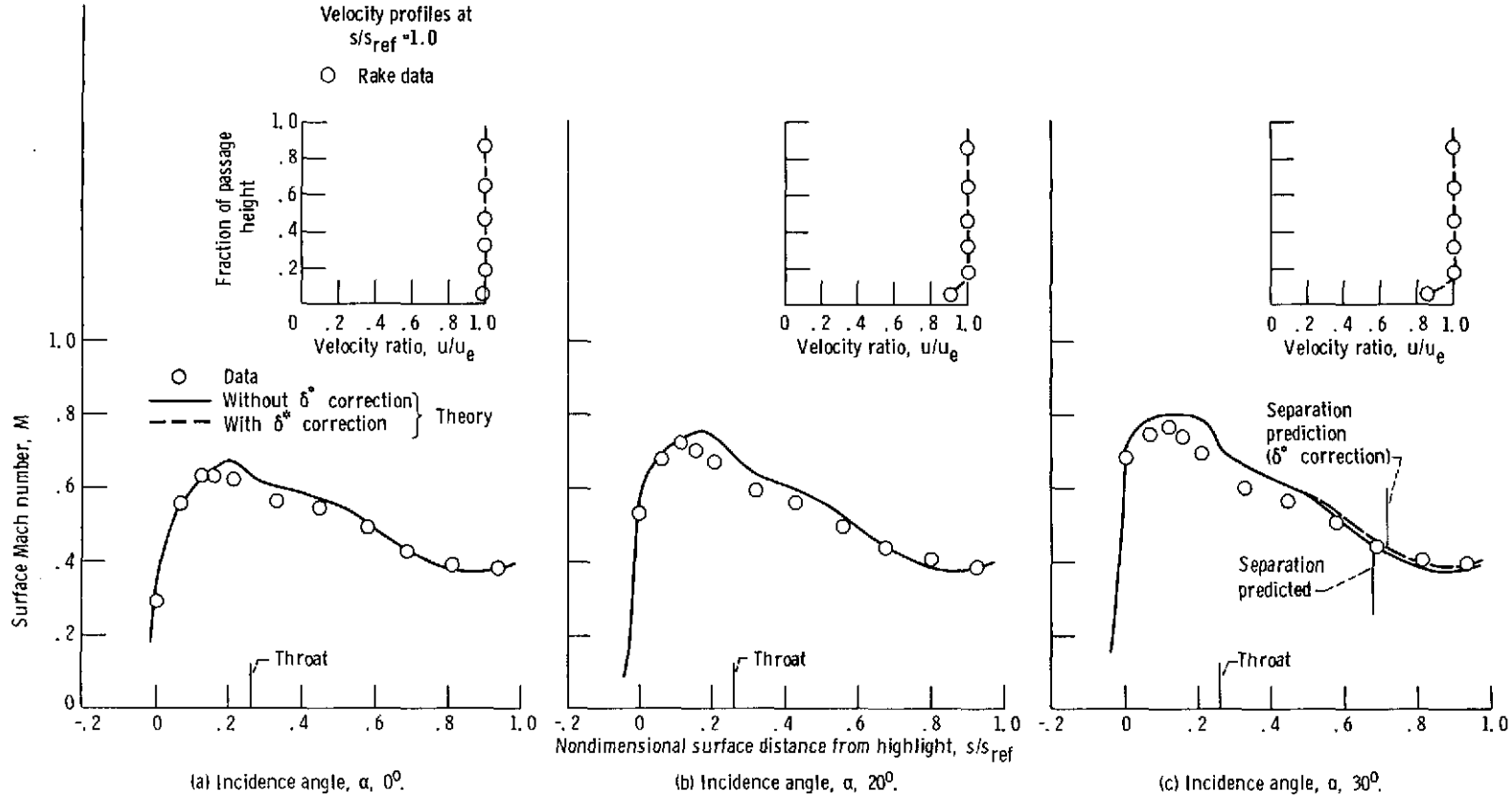

(a) Incidence angle, α, 0^0. (b) Incidence angle, α, 20^0. (c) Incidence angle, α, 30^0.

Figure 12. - Experimental and theoretical Mach number distributions and separation locations for centerbody extended, nonsymmetric lip; $\theta/2 = 5.3^0$ (configuration 4). One-dimensional throat Mach number, M_t, 0.534; free stream Mach number, M_∞, 0.127; windward side of inlet.

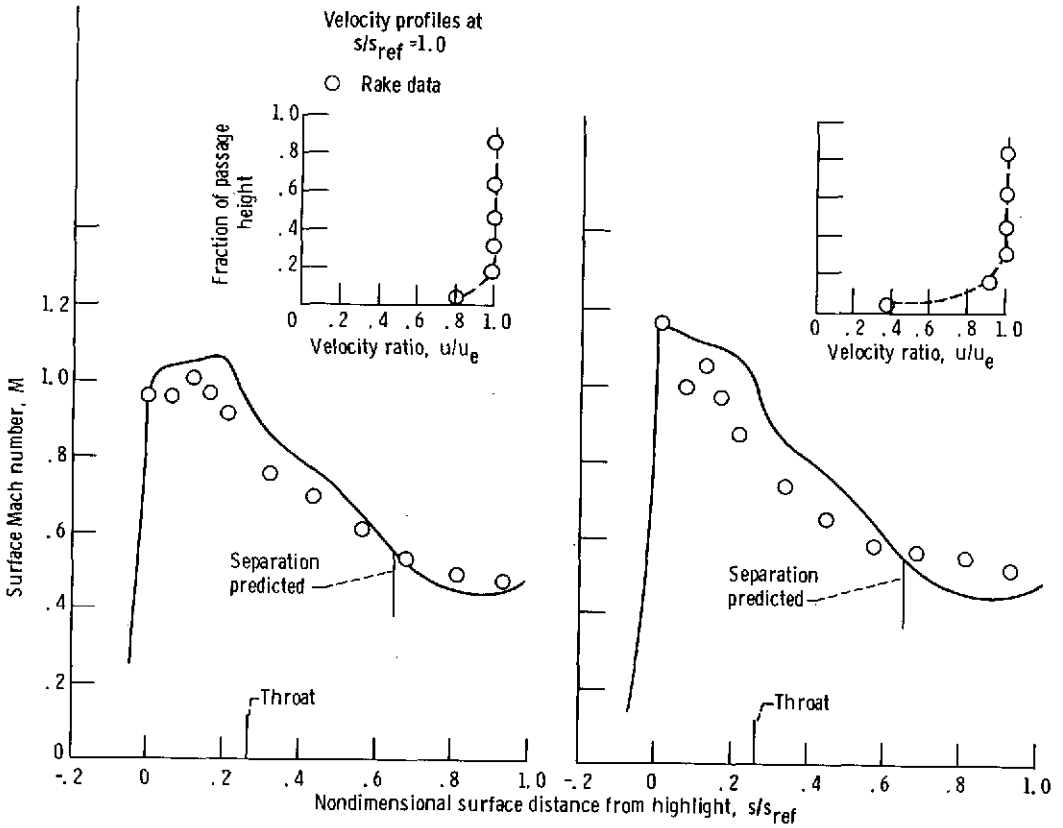

(d) Incidence angle, α, 40°.

(e) Incidence angle, α, 50°.

Figure 12. - Concluded.

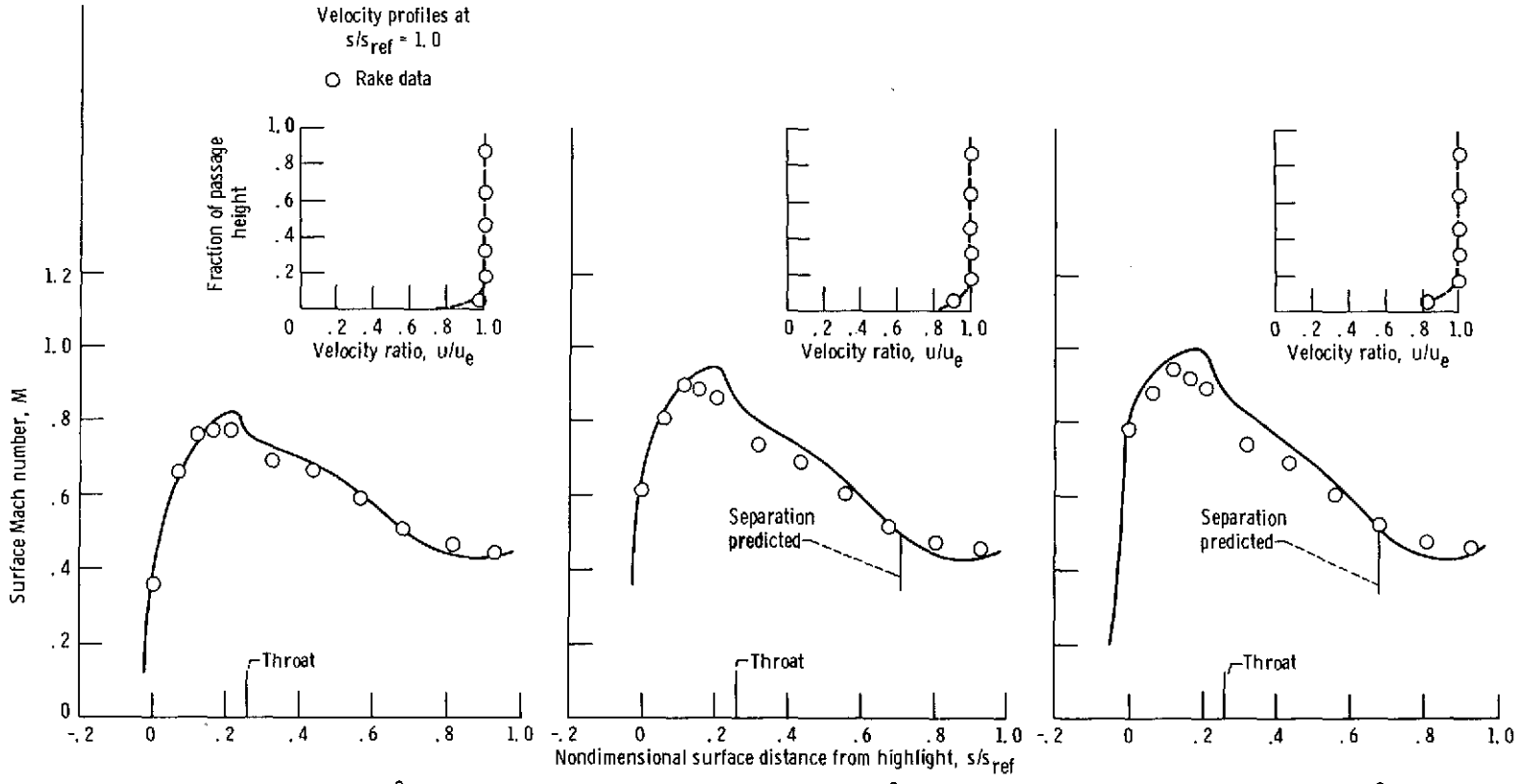

Figure 13. - Experimental and theoretical Mach number distributions and separation locations for centerbody extended, nonsymmetric lip; $\theta/2 = 5.3^{\circ}$ (configuration 4). ○ One-dimensional throat Mach number, M_t, 0.664; free stream Mach number, M_∞, 0.127; windward side of inlet.

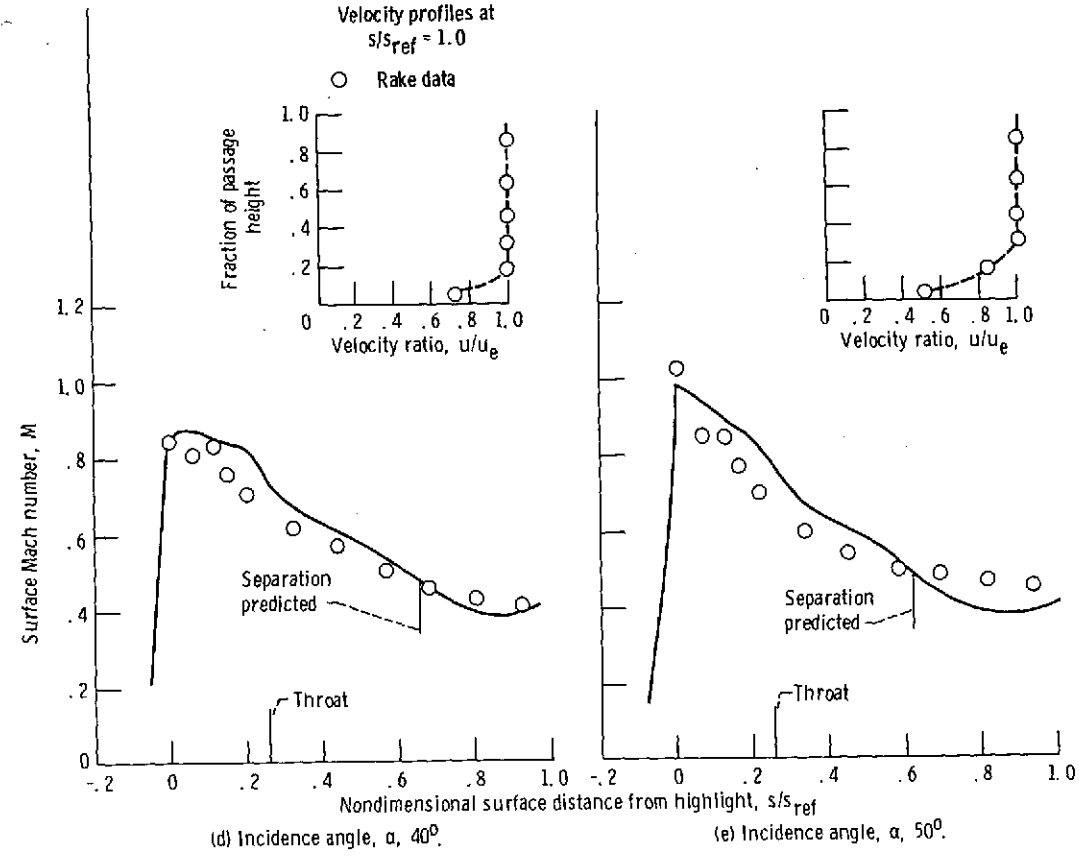

Figure 13. - Concluded.

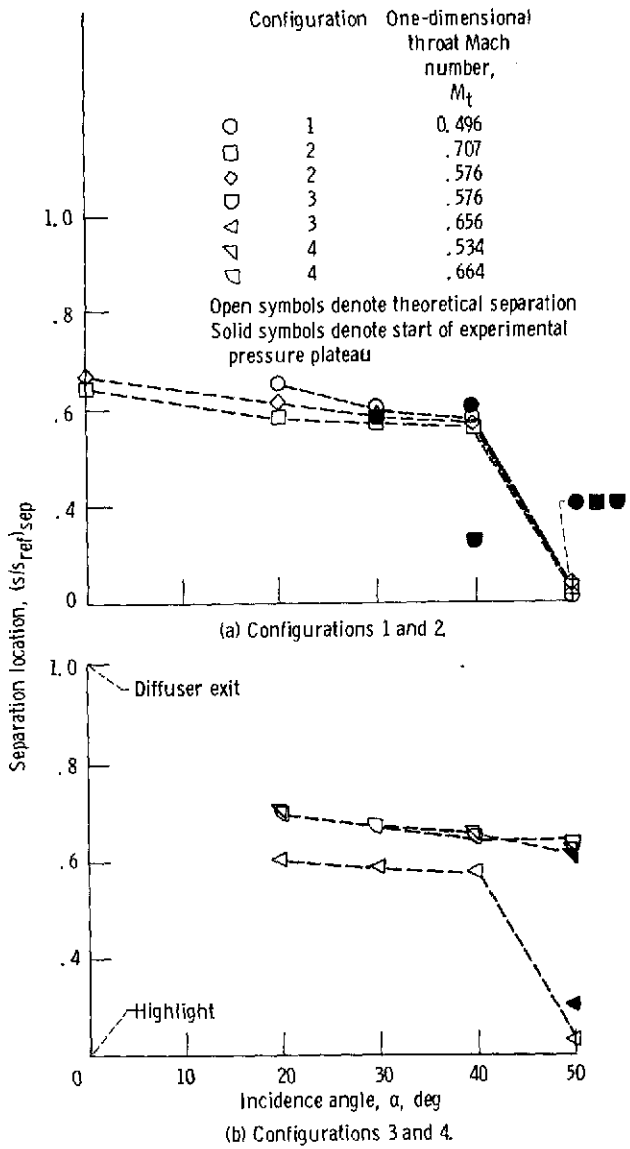

Figure 14. - Summary plot of separation locations (without δ^* correction).

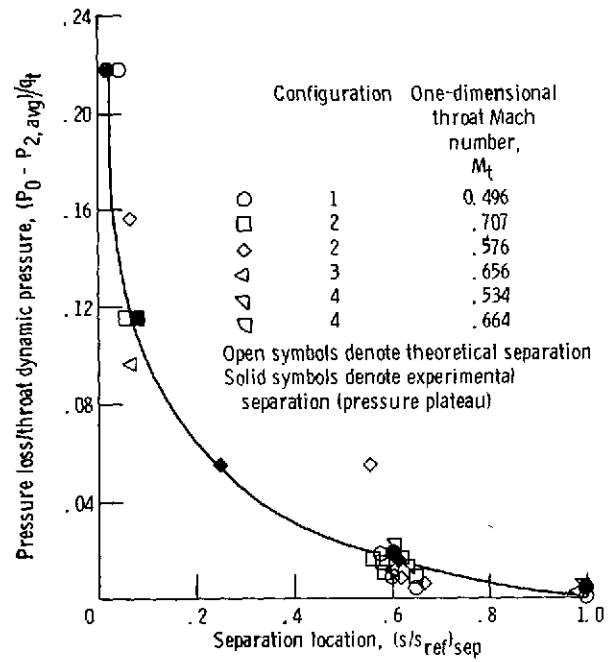

Figure 15. - Summary plot of relation of total pressure loss to separation locations.